



Modifying lewis base on TiO_2 nanosheets for enhancing CO_2 adsorption and the separation of photogenerated charge carriers

Zaiyong Jiang^{a,*}, Wenkang Miao^a, Xianglin Zhu^b, Guihua Yang^a, Zhimin Yuan^{a,*}, Jiachuan Chen^a, Xingxiang Ji^a, Fangong Kong^a, Baibiao Huang^{b,*}

^a State Key Laboratory of Biobased Material and Green Papermaking, Qilu University of Technology, Shandong Academy of Sciences, Jinan 250353, PR China

^b State key Laboratory of Crystal Materials, Shandong University, Jinan 250100, PR China



ARTICLE INFO

Keywords:

Lewis base
 $[\text{WO}_4]^{2-}$
 Photocatalytic CO_2 reduction
 CO_2 adsorption
 TiO_2

ABSTRACT

TiO_2 is one of the most studied in photocatalytic CO_2 field, while its efficiency was seriously limited by the weak adsorption ability for CO_2 and low separation efficiency of charge carriers. Here a lewis base $[\text{WO}_4]^{2-}$ was used to modify TiO_2 via an in-situ ion exchange strategy. It was found that the prepared samples showed better performance in CO_2 adsorption and carriers' separation. As a result, the $\text{TiO}_2/[\text{WO}_4]^{2-}$ composites had exhibited good activities in photocatalytic CO_2 reduction. The amount of generated CO was over 19 times that of the pure TiO_2 and it was even much better than precious metal (Ag, Au) modified TiO_2 . Our experiment proves that this kind of modifying Lewis base method is an efficient strategy for enhancing the CO_2 reduction activity of semiconductor photocatalysts.

1. Introduction

The development of the society is heavily dependent on the use of fossil fuels during the past hundred years which leads to the emissions of large amounts of CO_2 into the atmosphere. As a result, the global warming caused by the increasing CO_2 concentration in the air has become a serious problem that human must face. It has been a hotspot how to use CO_2 producing high valuable hydrocarbons productions like methanol (CH_3OH), methane (CH_4), carbon monoxide (CO), etc [1–4].

Now, photocatalytic CO_2 reduction has been proven efficient for the CO_2 conversion and utilization and shows tremendous potential for its intrinsic advantages. In the process of photocatalytic CO_2 , the reaction is usually carried out at ambient conditions; cheap semiconductor materials are used as catalysts and CO_2 and water are typically as the feedstock [5–10]. What's more, the only input energy comes from the solar in the reaction which makes it a green approach for CO_2 reduction. Although a large numbers of research work have been carried out, it is still a challenge to achieve high photocatalytic CO_2 reduction performance. Mainly because, CO_2 is a fully oxidized and thermodynamically stable molecular in the carbon recycling processes and it has been proven that large overpotentials must be overcome to finish the CO_2 reduction. Besides CO_2 as a linear and nonpolar gas molecule, it is difficult for the capture of CO_2 on the catalysts' surface sites which also influences the CO_2 reduction reaction.

Since 1978, Halmann et al. first report the photocatalytic reduction of CO_2 to produce chemical fuels by using a semiconductor photocatalyst [11]. To date, many semiconductors have been reported to drive the CO_2 conversion under solar irradiation, such as TiO_2 [12], Bi_2WO_6 [13], ZnS [14], GaN [15], C_3N_4 [16] and so on. Among of them, TiO_2 is one of the most studied photocatalysts in the CO_2 reduction field. TiO_2 has the band gaps around 3.0 eV–3.2 eV depending on the crystallographic phases. It is reported that CO_2 can be reduced to small molecules productions like CO, CH_4 and CH_3OH with using TiO_2 photocatalyst [17–19]. Though TiO_2 showed potential applications for CO_2 reduction, the efficiency of TiO_2 in CO_2 reduction is still very low and limited by wide band gap, the fast recombination of generated electrons and holes and the weak absorption for CO_2 . In view of the above-mentioned problem, several approaches have been developed to enhance the activity of TiO_2 .

Element doping were widely used and proven efficiently to expand the light absorption. Some elements like Fe, Co, Ni, Cu, N, C doped TiO_2 showed enhanced activity attributed to the shifts of absorption edge from UV to visible light region [20–25]. Besides, the construction of heterojunction could enhance the activity by promoting the carriers' separation on the surface of the catalysts. Typically, the enhancement of CO_2 adsorption can be realized by microstructure modulation. Utilizing the above approaches, the photocatalytic activity of TiO_2 in CO_2 reduction has been improved, while it is still far away from the practical

* Corresponding authors.

E-mail addresses: zaiyongjiang@qlu.edu.cn (Z. Jiang), yuanzhiminjinan@163.com (Z. Yuan), bbhuang@sdu.edu.cn (B. Huang).

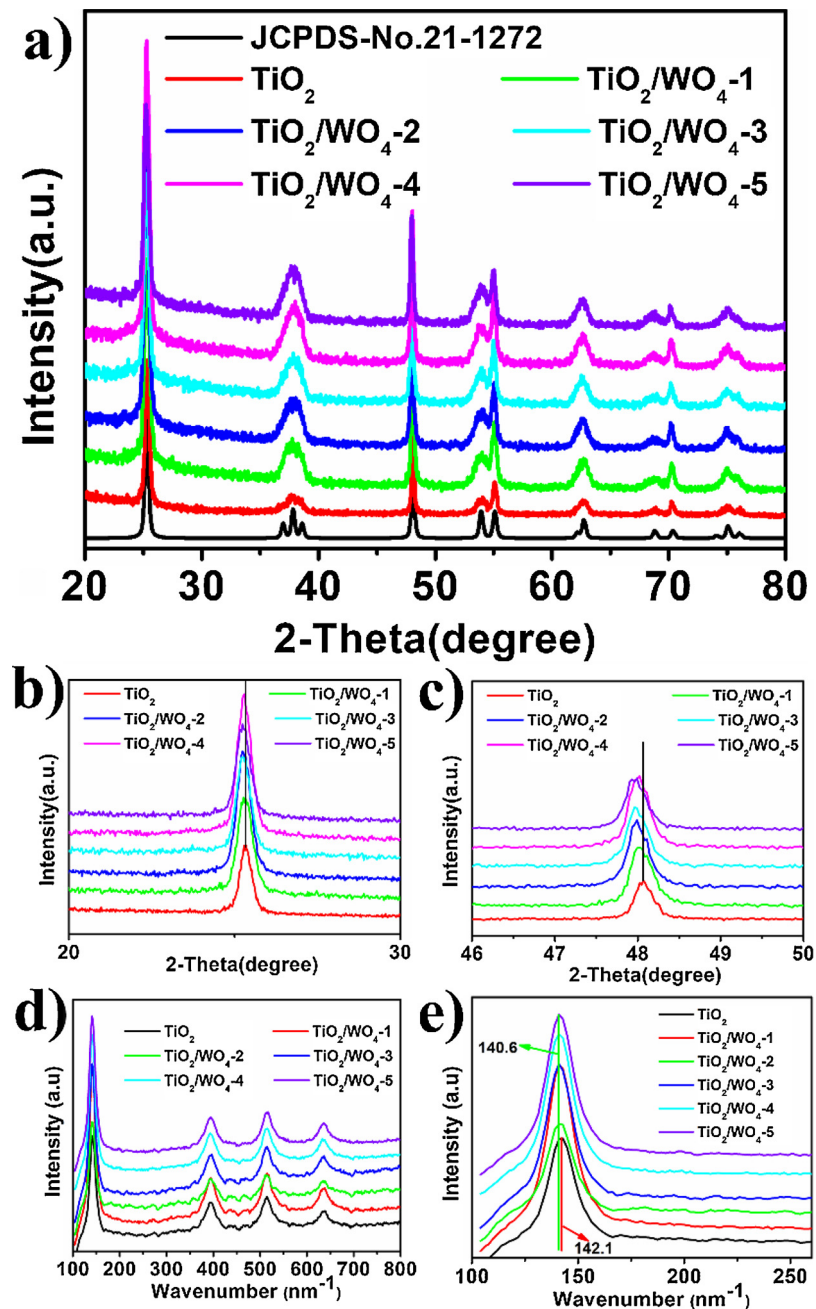


Fig. 1. (a), (b), (c) The XRD images and (d), (e) Raman spectra of samples.

application and much more efforts must be made.

Here, based on weak adsorption ability for CO_2 and low separation efficiency of charge carriers, we designed one kind of modified method to overcome the both limited problems. We modified TiO_2 nanosheets with $[\text{WO}_4]^{2-}$ through an in-situ ion exchange method which replaced the OH^- on the surface. As one kind Lewis base, the $[\text{WO}_4]^{2-}$ can enhance the absorption of the CO_2 which is very important for the CO_2 reduction. Meanwhile, our experiment results also proved that the modifying of $[\text{WO}_4]^{2-}$ improved the separation of the photo-generated carriers. As a result of enhanced CO_2 absorption and higher efficiency of carriers' separation, the $\text{TiO}_2/[\text{WO}_4]^{2-}$ (hereafter TiO_2/WO_4) showed better activity in photocatalytic CO_2 reduction compared with that of pristine TiO_2 .

2. Experimental

2.1. Synthesis of TiO_2 and TiO_2/WO_4 composite photocatalysts

The TiO_2 nanosheets were synthesized based on the literature [26]. The process of preparation was following: HF (3 mL) and 25 ml of tetrabutyl titanate were mixed together and continually stirred for 10 min. And then, the suspension was maintained in a 100 mL autoclave and kept at 200 $^\circ\text{C}$ for 24 h. The autoclave has been cooled to room temperature, the obtained sample has been washed by deionized water and absolute ethanol, respectively. The product was dried at 60 $^\circ\text{C}$ for 6 h in an oven.

A series of TiO_2/WO_4 composite photocatalysts have been obtained via a simple in-situ ion exchange method: (3 mg, 6 mg, 12 mg, 18 mg, 24 mg) $\text{Na}_2\text{WO}_4 \cdot 2\text{H}_2\text{O}$, (0.1 g) TiO_2 and 100 ml deionized water were mixed together and continually stirred for 4 h. And then, the

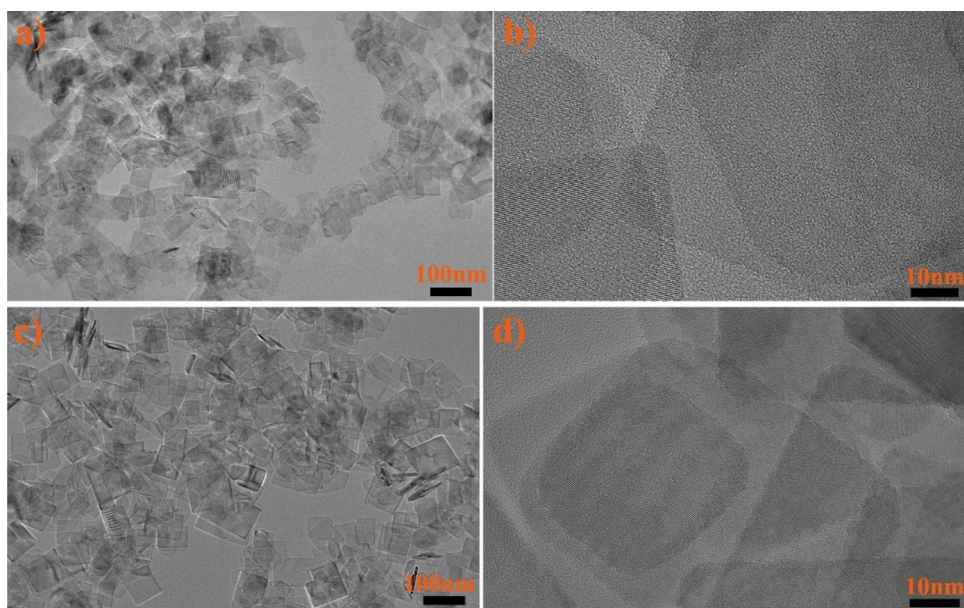


Fig. 2. HRTEM images (a, b) TiO_2 and (c, d) $\text{TiO}_2/\text{WO}_4\text{-}3$.

corresponding products were filtered and washed, and noted as $\text{TiO}_2/\text{WO}_4\text{-}1$, $\text{TiO}_2/\text{WO}_4\text{-}2$, $\text{TiO}_2/\text{WO}_4\text{-}3$, $\text{TiO}_2/\text{WO}_4\text{-}4$ and $\text{TiO}_2/\text{WO}_4\text{-}5$. After that, the obtained TiO_2/WO_4 was dried at 60 °C in an oven.

2.2. Characterization

The obtained products have been analyzed via X-ray powder diffraction (XRD) on a Bruker AXS D8 advance powder diffractometer. Raman spectra were recorded on LABRAM-HR800 system with laser excitation of 633 nm. The morphologies and chemical composition of the products were confirmed by SEM and EDS using a Hitachi S-4800 microscope. High-resolution transmission electron microscopy (HRTEM) measurements were performed by a JEOL-2100 microscope. The UV-vis diffuse reflectance spectra were carried out on a Shimadzu UV 2550 recording spectrophotometer, which is equipped with an integrating sphere with BaSO_4 as a reference. X-ray photoelectron spectroscopy (XPS) was performed using a Thermo Fisher Scientific (ESCALAB 250) X-ray photoelectron spectrometer and the result was charge corrected to the adventitious C 1s peak at 284.6 eV. The PL measurements were carried out on a Hitachi F-4500 fluorescence spectrophotometer under 320 nm excitation. A Micromeritics ASAP 2020 analyzer was used to measure the Brunauer-Emmett-Teller (BET) surface areas of the samples at liquid nitrogen temperature.

2.3. Photocatalytic CO_2 reduction evaluation

The procedure of CO_2 photoconversion is the following: The sample (0.1 g) was dispersed into 100 mL H_2O with vigorous stirring, subsequently, continuously bubbled via high purity CO_2 gas for 15 min. The light source was a 300 W Xe arc lamp (PLS-SXE300, Beijing Trusttech Co., Ltd.). The temperature of reactor was controlled at 15 °C by cooling water circulation equipment. At the given time interval, the gas was got out and monitored via Varian CP-3800 gas chromatograph (FID detector, Propark Q column).

3. Results and discussion

Firstly, the crystalline structures of the as-prepared samples were characterized in detail via powder XRD and the results were shown in Fig. 1a–c. Fig. 1a showed the diffraction peaks of all samples including the pristine TiO_2 correspond well with the anatase TiO_2 structure

(JCPDS no. 21-1272). And no any impurity peaks (such as WO_3 , $\text{W}_{18}\text{O}_{49}$, etc) were observed. In addition, with the increase of concentrations of $\text{Na}_2\text{WO}_4\cdot 2\text{H}_2\text{O}$, it is found in Fig. 1b,c the peaks attached to (101) and (200) facets shifted toward low degree, which could be due to the effect of surface stress after the introduction of $[\text{WO}_4]^{2-}$. The result indicated the designed modification maybe be realized. Analysis of Raman spectra were performed to further support the XRD results. As shown in Fig. 1d, both pristine TiO_2 and TiO_2/WO_4 displayed typical anatase Raman bands. The peaks at 142, 394, 513 and 639 cm^{-1} are attributed to the E_g , B_{1g} , A_{1g} and E_g modes of anatase phase of TiO_2 , respectively [27,28]. In addition, there was an obvious shift about E_g mode of TiO_2/WO_4 composites compared with that of pristine TiO_2 in Fig. 1e, implying various defects or the effect of surface stress of TiO_2/WO_4 . Moreover, Fig. S1 exhibited that the suspension solution of TiO_2/WO_4 composites and pristine TiO_2 in water was obvious different, the TiO_2/WO_4 suspension solution looked like colloidal solution, not easily sank. In order to explore the reason, the zeta potentials of TiO_2 and TiO_2/WO_4 nanosheets were measured. And the value is -2.12, -5.68, -15.90, -23.10, -32.92, -39.01, respectively. It is very obvious that the value became more and more negative with the increase of introduction amount of $[\text{WO}_4]^{2-}$, perfectly explaining the reason about colloidal solution. These results of suspension solution and zeta potentials corresponded to the XRD and Raman spectra, further confirming the introduction of $[\text{WO}_4]^{2-}$.

The morphologies of prepared TiO_2 and TiO_2/WO_4 were characterized by SEM. As shown in Fig. S2, we can conclude that both samples possess uniform nanosheets morphology, and no significant difference between pristine TiO_2 and TiO_2/WO_4 is observed. The surface states of pristine TiO_2 and $\text{TiO}_2/\text{WO}_4\text{-}3$ sample were further investigated using HRTEM and the results were shown in the Fig. 2. It can be observed that the average length and width of the nanosheets of both samples is about 50 nm, 30 nm, respectively. There is also no obvious different to be found. These results indicated that the modification of $[\text{WO}_4]^{2-}$ is achieved, not forming the heterojunction. The distribution of the surface elements was analyzed with EDS mapping technology and the results were shown in Fig. S3, S4. From Fig. S3 we can see that the W element showed similar distribution trends compared with Ti and O, and this indicated the W was uniformly modified on the surface of TiO_2 . From Fig. S4, the amount of the $[\text{WO}_4]^{2-}$ on the surface was calculated and the atomic ratios of W/Ti on the surface were about 0.5% ($\text{TiO}_2/\text{WO}_4\text{-}1$), 0.9% ($\text{TiO}_2/\text{WO}_4\text{-}2$), 2.1% ($\text{TiO}_2/\text{WO}_4\text{-}3$), 2.5% ($\text{TiO}_2/\text{WO}_4\text{-}4$)

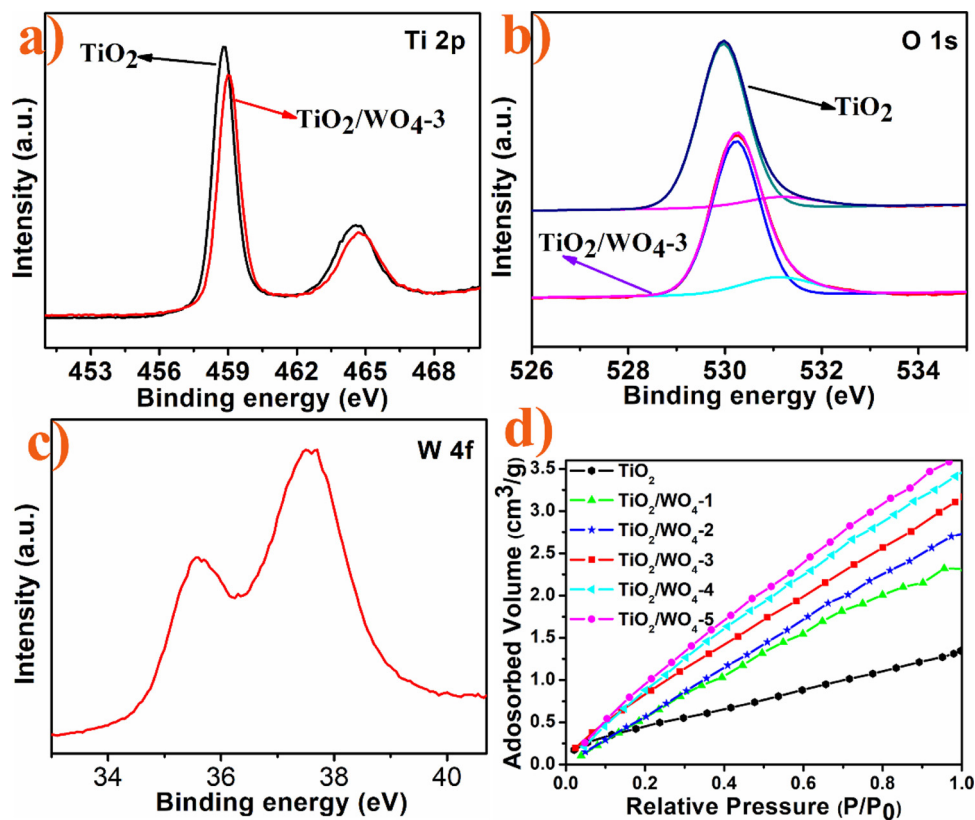


Fig. 3. XPS spectra of TiO₂/WO₄-3 and TiO₂: (a) the Ti 2p, (b) the O 1s and (c) the W 4f; (d) Adsorption isotherms of TiO₂ and TiO₂/WO₄-3 products at 298 K about CO₂.

and 3.2% (TiO₂/WO₄-5), respectively.

To identify the valence states of the W ions and the chemical composition of the deposited samples, TiO₂/WO₄-3 sample chosen as an example was analyzed through XPS. For comparison, pristine TiO₂ sample was also investigated. And the high resolution XPS spectra of the Ti 2p (Fig. 3a), O1s (Fig. 3b) and Ti 2p (Fig. 3c) binding energy regions are shown in Fig. 3. As shown in Fig. 3a,b, both samples exhibited similar Ti 2p and O1s XPS peaks, but there is a small shift towards the higher binding energy in TiO₂/WO₄-3 sample compared to that of pristine TiO₂. The change of XPS indicated the modification of [WO₄]²⁻ was not only a physical adsorption and a new chemical binding was formed between Ti⁴⁺ and [WO₄]²⁻ through ion exchange with OH⁻. Furthermore, there are two peaks centered at 35.6 and 37.6 eV in TiO₂/WO₄-3 sample (Fig. 3c), which are assigned to the W 4f_{7/2} and W 4f_{5/2} featuring W⁶⁺. CO₂ adsorption isotherms have been carried out at 298 K and 1 atm. As shown in Fig. 3d, TiO₂/WO₄ samples showed much higher CO₂ adsorption capacity compared to that of pure TiO₂. The above CO₂ adsorption results proved that the introduction of [WO₄]²⁻ can increase the CO₂ adsorption capacity of TiO₂ nanosheets. Furthermore, we have chosen the TiO₂/WO₄-3 as a sample to investigate the N₂-adsorption isotherm. For comparison, pristine TiO₂ has also been studied and the corresponding BET curves have been exhibited in Fig. S5. The BET surface areas of pristine TiO₂ and TiO₂/WO₄-3 were 73.4 and 82.79 m²/g (TiO₂/WO₄-3), respectively, only a small change. The result suggested that the enhancement of CO₂ adsorption capacity mainly derived from the introduction of lewis base [WO₄]²⁻ to coupling the lewis acid (CO₂), rather than the change of BET surface areas. Simultaneously indicating that TiO₂/WO₄-3 would perform better for CO₂ photoconversion than pristine TiO₂. The absorption spectra of TiO₂ and TiO₂/WO₄ samples were characterized and the results were shown in Fig. S6a. It was observed that the absorption band edge of TiO₂/WO₄ was slightly red shifted compared to that of pristine TiO₂. Moreover, the photoluminescence (PL) spectra of TiO₂

and TiO₂/WO₄ were performed. As shown in Fig. S6b, the position of the emission peak of all samples was similar, but the intensities of TiO₂/WO₄ are obviously lower than that of pristine TiO₂. This result suggests that TiO₂/WO₄ possesses a much lower recombination rate of photo-generated charge carriers, compared to pristine TiO₂ [29]. The PL intensities of TiO₂/WO₄ decrease, suggesting the [WO₄]²⁻ plays an important role in separation efficiency of photo-generated electrons and holes.

For semiconductor photocatalysts, most of photogenerated charge carriers can't separate timely due to poor conductivity. Here, we have checked the sample conductivities by using electrochemical impedance spectroscopy (EIS). According to Fig. 4a, the TiO₂/WO₄ samples presented a much smaller radius than the pure TiO₂ sample, which suggested better conductivity and this was beneficial to the photocatalytic activities. Besides, in the photoelectrochemical tests (Fig. 4b), the TiO₂/WO₄ sample shows much higher photocurrent intensity than the pure TiO₂, which also indicated the higher efficiency of carriers [30]. Among them, the TiO₂/WO₄-3 sample exhibited the best performance toward EIS and photocurrent intensity.

Based on above discussion, it is found that TiO₂/WO₄ has improved CO₂ adsorption capacity and more efficient separation of photo-generated electrons and holes compared to that of pristine TiO₂. Therefore, they should exhibit higher photocatalytic CO₂ activities than TiO₂. In order to confirm the fact, the photocatalytic activities of as prepared samples were performed. For comparison, pristine TiO₂, Au/TiO₂ and Ag/TiO₂ samples were carried out the photocatalytic CO₂ reduction experiment. As shown in Fig. 4c, the photocatalytic CO₂ reduction activities for TiO₂/WO₄ samples were prominently improved toward CO production compared to pristine TiO₂. Among them, the TiO₂/WO₄-3 has displayed the highest activity of CO₂ photoconversion after 2 h irradiation, in which the relative reaction rate is about 19 times (CO) higher than that of the pristine TiO₂. It is worth noting that the TiO₂/WO₄ sample showed much better activity compared with Ag/TiO₂ and

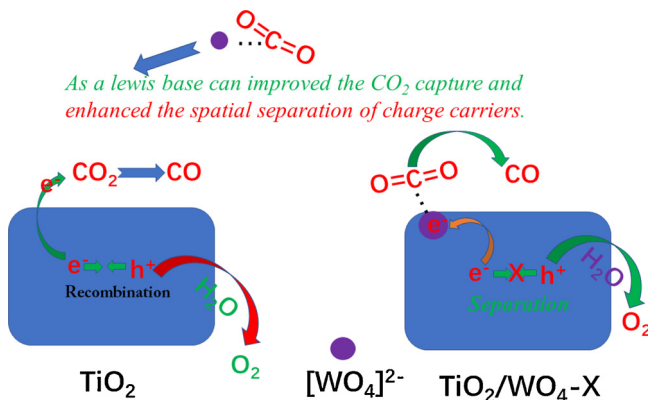
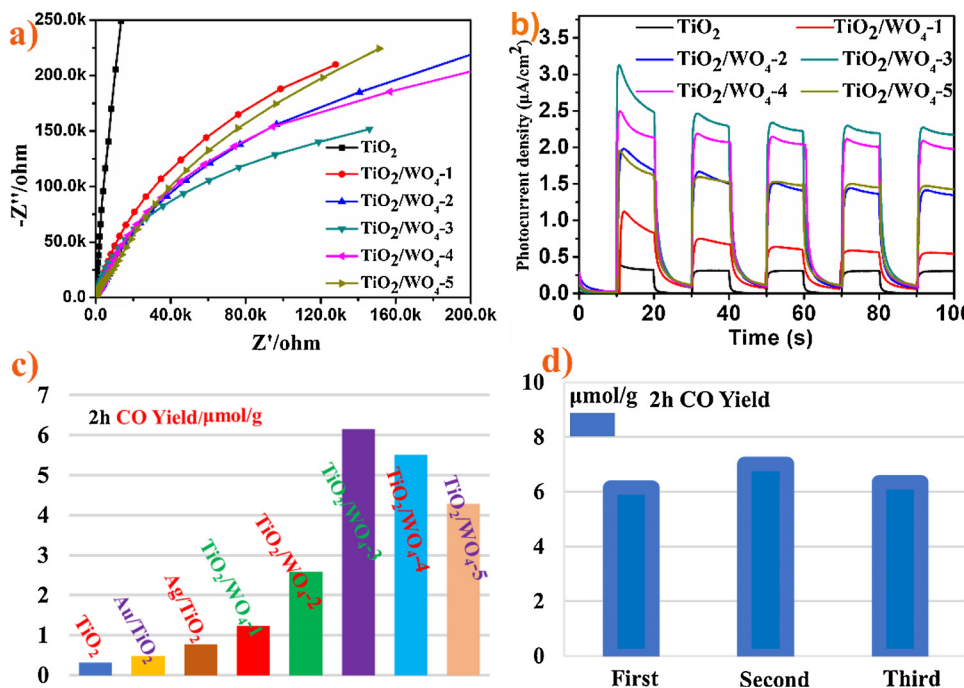


Fig. 5. The mechanism of photocatalytic CO_2 reduction with TiO_2 and TiO_2/WO_4 .

Au/TiO_2 and this also indicated the key role of $[\text{WO}_4]^{2-}$ in the TiO_2/WO_4 composites for photocatalytic CO_2 reduction. In addition, except for CO during photocatalytic CO_2 reduction, we have also detected a small amount of CH_4 (Fig. S7). The stability test results were given in Fig. 4d. There was no obvious decay after three cycles' test and it proved the good stability of the TiO_2/WO_4 -3 catalyst.

Combining the above discussion, we proposed a possible reaction mechanism of enhanced photocatalytic CO_2 reduction with TiO_2/WO_4 , which were shown in Fig. 5. The $[\text{WO}_4]^{2-}$ was fixed on the surface of the TiO_2 through in-situ exchanging OH^- . As a lewis base, $[\text{WO}_4]^{2-}$ enhanced the capture of CO_2 on the surface of catalyst compared with that of pristine TiO_2 . Besides, TiO_2 and TiO_2/WO_4 could be excited to generate electrons (e^-) and holes (h^+) via the effect of UV-vis light irradiation. As the pristine TiO_2 , the photogenerated e^- was transferred to the CBM to reduce adsorbed CO_2 molecules to CO gas. However, the photo-generated electrons of TiO_2/WO_4 will be trapped by the $[\text{WO}_4]^{2-}$, thereby realizing the more efficient separation of charge carriers, simultaneously reducing adsorbed CO_2 molecules to CO gas. On the other hand, the more h^+ could oxidize water molecules giving rise to O_2 compared to that of pristine TiO_2 . Moreover, the enhancement of the CO_2 adsorption capacity may provide more CO_2 gas to participate in the CO_2 reduction reaction, thereby obtaining high CO_2 photoconversion

Fig. 4. (a) Electrochemical impedance spectroscopy of TiO_2 and TiO_2/WO_4 under UV-vis light illumination, and the electrolyte solution was 0.2 M Na_2SO_4 aqueous solution; (b) Photocurrent intensity of TiO_2 and TiO_2/WO_4 at 0.2 V under UV-vis light illumination; (c) CO yield of the samples during the 2 h light irradiation; (d) Repeated photocatalytic CO_2 reduction activity producing CO of TiO_2/WO_4 -3 sample.

rate. That is to say, the enhanced photocatalytic activity of TiO_2/WO_4 compared with that of pristine TiO_2 can be ascribed to the more efficient separation of photo-generated charge carrier and the enhanced CO_2 adsorption capacity.

4. Conclusions

In summary, we have prepared TiO_2/WO_4 photocatalysts through modifying TiO_2 nanosheets with lewis base ($[\text{WO}_4]^{2-}$) by the in-situ ion exchange method. The fixed $[\text{WO}_4]^{2-}$ enhanced the ability of capturing CO_2 . What's more the modifying of $[\text{WO}_4]^{2-}$ can help promote the separation of charge carriers. In photocatalytic CO_2 reduction experiments, TiO_2/WO_4 photocatalysts showed much better activity compared to pure TiO_2 and precious metal (Ag and Au) modified TiO_2 . Based on the results of this study, we can conclude that this kind of modifying Lewis base approach maybe an efficient method to improve photocatalytic CO_2 reduction.

Declarations of interest

None.

Acknowledgments

This work was financially supported by a research Grant from the National Key Research and Development Program of China (Grant No. 2017YFB0307900), the Natural Science Foundation of Shandong Province, China (ZR2018BB042), the National Natural Science Foundation of China (Grant Nos.31670595,31770628) and the Taishan Scholars Program.

Appendix A. Supplementary data

Supplementary material related to this article can be found, in the online version, at doi:<https://doi.org/10.1016/j.apcatb.2019.117881>.

References

[1] L. Wang, M. Ghoussoub, H. Wang, Y. Shao, W. Sun, A.A. Tountas, T.E. Wood, H. Li, J.Y.Y. Loh, Y.C. Dong, M.K. Xia, Y. Li, S.H. Wang, J. Jia, C.Y. Qiu, C.X. Qian,

N.P. Kherani, L. He, X.H. Zhang, G.A. Ozin, Joule 2 (2018) 1–13.

[2] P.G. O'Brien, A. Sandhel, T.E. Wood, A.A. Jelle, L.B. Hoch, D.D. Perovic, C.A. Mims, G.A. Ozin, Adv. Sci. 1 (2014) 1400001.

[3] H.M. Liu, H. Song, W. Zhou, X.G. Meng, J.H. Ye, Angew. Chem. Int. Ed. 57 (2018) 16781–16784.

[4] G.B. Chen, R. Gao, Y.F. Zhao, Z.H. Li, G.I.N. Waterhouse, R. Shi, J.Q. Zhao, M.T. Zhang, L. Shang, G.Y. Sheng, X.P. Zhang, X.D. Wen, L.Z. Wu, C.H. Tung, T.R. Zhang, Adv. Mater. 30 (2018) 1704663.

[5] G.H. Yang, W.K. Miao, Z.M. Yuan, Z.Y. Jiang, B.B. Huang, P. Wang, J.C. Chen, Appl. Catal. B: Environ. 237 (2018) 302–308.

[6] J.G. Hou, H.J. Cheng, O. Takeda, H.M. Zhu, Angew. Chem. Int. Ed. 54 (2015) 8480–8484.

[7] M.C. Gao, J.X. Yang, T. Sun, Z.Z. Zhang, D.F. Zhang, H.J. Huang, H.X. Lin, Y. Fang, X.X. Wang, Appl. Catal. B: Environ. 243 (2019) 734–740.

[8] X. Liu, S.J. Inagaki, J.L. Gong, Angew. Chem. Int. Ed. 55 (2016) 14924–14950.

[9] Y.M. He, L.H. Zhang, B.T. Teng, M.H. Fan, Environ. Sci. Technol. 49 (2015) 649–656.

[10] C.D. Windle, E. Pastor, A. Reynal, A.C. Whitwood, Y. Vaynzof, J.R. Durrant, R.N. Perutz, E. Reisner, Chem-Eur. J. 21 (2015) 3746–3754.

[11] M. Halmann, Nature 275 (1978) 115–116.

[12] Z.Y. Jiang, X.H. Zhang, Z.M. Yuan, J.C. Chen, B.B. Huang, D.D. Dionysiou, G.H. Yang, Chem. Eng. J. 348 (2018) 592–598.

[13] S.W. Cao, B.J. Shen, T. Tong, J.W. Fu, J.G. Yu, Adv. Funct. Mater. 28 (2018) 1800136.

[14] X.G. Meng, Q. Yu, G.G. Liu, L. Shi, G.X. Zhao, H.M. Liu, P. Li, K. Chang, T. Kako, J.H. Ye, Nano Energy 34 (2017) 524–532.

[15] B. Alotaibi, S.Z. Fan, D.F. Wang, J.H. Ye, Z.T. Mi, ACS Catal. 5 (2015) 5342–5348.

[16] S.B. Wang, Y.D. Hou, X.C. Wang, ACS Appl. Mater. Interfaces 7 (2015) 4327–4335.

[17] Q. Kang, T. Wang, P. Li, L.Q. Liu, K. Chang, M. Li, J.H. Ye, Angew. Chem. Int. Ed. 127 (2015) 855–859.

[18] M. Tahir, N.S. Amin, Appl. Catal. B: Environ. 162 (2015) 98–109.

[19] S.M. Park, A. Razzaq, Y.H. Park, S. Sorar, Y. Park, C.A. Grimes, S. In, ACS Omega 1 (2016) 868–875.

[20] W.R. Zhao, J. Zhang, X. Zhu, M. Zhang, J. Tang, M. Tan, Y. Wang, Appl. Catal. B: Environ. 144 (2014) 468–477.

[21] M.Y. Xing, D.Y. Qi, J.L. Zhang, F. Chen, Chem-Eur. J. 17 (2011) 11432–11436.

[22] D.M. Chen, Z.Y. Jiang, J.Q. Geng, Q. Wang, D. Yang, Ind. Eng. Chem. Res. 46 (2007) 2741–2746.

[23] M.A. Barakat, H. Schaeffer, G. Hayes, S. Ismat-Shah, Appl. Catal. B: Environ. 1 (2005) 23–30.

[24] Q. Liu, D.Y. Ding, C.Q. Ning, X.W. Wang, Int. Hydrogen Energy 40 (2015) 2107–2114.

[25] T.D. Pham, B.K. Lee, Chem. Eng. J. 286 (2016) 377–386.

[26] J.G. Yu, J.X. Low, W. Xiao, P. Zhou, M. Jaroniec, J. Am. Chem. Soc. 136 (2014) 8839–8842.

[27] X. Chen, P.Y. Yu, S.S. Mao, Science 331 (2011) 746–750.

[28] X. Pan, M.Q. Yang, X. Fu, N. Zhang, Y.-J. Xu, Nanoscale 5 (2013) 3601–3614.

[29] J. Di, J.X. Xia, S. Yin, H. Xu, L. Xu, Y.G. Xu, M.Q. He, H.M. Li, RSC Adv. 4 (2014) 14281–14290.

[30] Q.W. Huang, S.Q. Tian, D.W. Zeng, X.X. Wang, W.L. Song, Y.Y. Li, W. Xiao, C.S. Xie, ACS Catal. 3 (2013) 1477–1485.